IAHR AIRH
Taylor & Francis
Taylor & Francis Group

Journal of Hydraulic Research Vol. 50, No. 4 (2012), pp. 353–363
http://dx.doi.org/10.1080/00221686.2012.686200

Research paper

Undular and breaking bores on fixed and movable gravel beds

NAZANIN KHEZRI, *School of Civil Engineering, The University of Queensland, St Lucia, Brisbane, Qld. 4072, Australia.*
Email: n.khezri@uq.edu.au

HUBERT CHANSON (IAHR Member), *School of Civil Engineering, The University of Queensland, St Lucia, Brisbane, Qld. 4072, Australia.*
Email: h.chanson@uq.edu.au (author for correspondence)

ABSTRACT
A tidal bore is a positive surge taking place during the flood tide with a large tidal range and the bore corresponds to the leading edge of the tidal wave propagating upstream. In this study, some physical modelling was performed to investigate the upstream bore propagation over fixed and movable gravel beds. Both undular and breaking bores were tested. The free-surface and velocity measurements were complemented by some observations of particle motion beneath the bore front. In the initially-steady flow and beneath undular bores, no sediment motion was observed for the experimental set-up. Beneath breaking bores, on the other hand, some upstream gravel bed load motion was observed behind the bore. The gravel bed particles were de-stabilized by the roller toe passage and advected upstream. The unsteady velocity data showed some damping of the transient recirculation on the movable gravel bed.

Keywords: Movable bed; physical modelling; tidal bores; turbulent flow properties; unsteady flow measurements

1 Introduction

A tidal bore is a series of waves propagating upstream in a river mouth as the tide starts to rise (Rayleigh 1908, Peregrine 1966). The existence of the bore is associated with a large tidal range amplified by the estuarine bathymetry and relatively low freshwater levels to fulfil momentum considerations (Darwin 1897, Tricker 1965). The bore constitutes a discontinuity in water depth at the bore front. Figure 1 shows a breaking tidal bore in the Bay of Mont Saint Michel in western France. The flow properties immediately in front of and behind the bore must satisfy the continuity and momentum principles (Henderson 1966, Liggett 1994, Chanson 2012). The shape of the bore is characterized by its Froude number F defined for a rectangular channel as:

$$\mathsf{F} = \frac{V_0 + U}{\sqrt{g\ d_0}} \tag{1}$$

where V_0 is the initial river flow velocity positive downstream, U is the tidal bore celerity for an observer standing on the bank positive upstream, g is the gravity acceleration and d_0 is the initial river flow depth. For $1 < \mathsf{F} < 1.4$–1.6, the tidal bore leading edge is followed by a train of secondary waves, i.e. an undular bore (Treske 1994, Koch and Chanson 2008). For larger Froude numbers, a breaking tidal bore is observed (Fig. 1).

Some studies investigated the unsteady turbulence induced by the bore (Hornung *et al.* 1995, Koch and Chanson 2009, Chanson and Tan 2010) and the results highlighted the intense mixing beneath the bore front. These findings were consistent with field observations of bed erosion and upstream sediment advection (Chen *et al.* 1990, Tessier and Terwindt 1994, Chanson *et al.* 2011), although laboratory studies until now were conducted with fixed bed. A number of studies highlighted some key differences between fixed bed and movable bed hydraulics in steady open channel flow (Graf 1971, Nikora and Goring 2000). Some results implied a greater turbulence anisotopy in the presence of mobile bed (Nikora and Goring 2000) with a damping of near-bed turbulence (Dey *et al.* 2011). To date, however, no systematic study was performed in highly-unsteady open channel flows. In this study, the turbulent velocity fields of breaking and undular bores were investigated physically on both fixed gravel bed and movable gravel bed. The experimental study was based upon a Froude dynamic similarity, and some turbulent velocity measurements were conducted with a relatively high-temporal and spatial

Revision received 30 November 2011/Open for discussion until 28 February 2013.

ISSN 0022-1686 print/ISSN 1814-2079 online
http://www.tandfonline.com

Figure 1 Photograph of the breaking tidal bore of the Sélune River on 24 September 2010 in Bay of Mont Saint Michel (France) – bore propagating from right to left

resolution for a number of Froude numbers to provide some Eulerian description of the turbulent flow field. Some sediment tracking under both breaking and undular bores complemented the study to characterize the bed load motion beneath the tidal bore front.

2 Experimental facilities

The experiments were performed in a rectangular channel, 0.5 m wide and 12 m long, made of smooth PVC bed and glass walls. A fast closing tainter gate was located at $x = 11.15$ m, where x is the longitudinal distance from the channel upstream and positive downstream. The tainter gate could be closed rapidly, completely or partially, to generate a tidal bore propagating upstream into the channel.

Two orifice meters, designed based on British Standards (British Standard 1943), were used to record the initially-steady discharge. The steady flow depths were measured using rail-mounted pointer gauges. All the water depths were measured above the top of the gravel bed using a semi-circular footing with a 25.1 cm^2 area. Four–six acoustic displacement metres Microsonic™ Mic+25/IU/TC were installed between $x = 4$ and 10.8 m above the water surface to detect non-intrusively the water elevation fluctuations. The response time of the displacement meters was less than 20 ms and their vertical accuracy was 0.18 mm.

An acoustic Doppler velocimeter (ADV) Nortek™ Vectrino+ was installed at $x = 5$ m to measure the turbulent velocity fluctuations. The ADV system was equipped with a three-dimensional side looking head. The time and velocity resolutions of the ADV unit were, respectively, 5 ms and 1 cm/s. The ADV data were post-processed using the software WinADV™. In steady flows, some phase-space threshold despiking and the removal of communication errors, low signal-to-noise ratios and low correlations were performed. For the unsteady flows, only the removal of communication errors and a replacement by linear interpolation were conducted since the other forms of post-processing were never validated in highly-unsteady flows.

During all experiments, the observations were conducted between $x = 4$ and 6 m and some video movies were recorded with a digital video camera Panasonic™ NV-GS300 (25 fps).

2.1 *Gravel bed configurations*

For all the experiments, the original channel PVC bed was covered with a series of plywood sheets, 1.2 m long and 0.5 m wide, covered by natural gravels (relative density $\rho_s/\rho = 2.65$) sieved between 4.75 and 6.70 mm, glued in resin and covered by a spray gloss surface finish. This set-up was the fixed gravel bed configuration. In a second set-up, a 1 m long section of smooth-painted plywood sheet was installed beneath the study region ($4.5 < x < 5.5$ m) and a layer of loose gravels was spread evenly prior to the beginning of each experiment. Some particles were coloured to facilitate the video-record analyses. The same gravel material was used for the fixed and movable beds.

The roughness of fixed gravel bed was assessed for a range of steady flow conditions ($0.01 < Q < 0.07$ m^3/s and $0.06 < d_0 < 0.17$ m). The results yielded a Darcy–Weisbach friction factor between $f = 0.031$ and 0.045, corresponding to an equivalent sand roughness height of 3.4 mm comparable to the median gravel size of 5.7 mm.

The sediment material and its properties (density, size) were selected to observe no sediment motion in the initially-steady flow and some onset of sediment transport during bore propagation. It will be shown that sediment motion was only observed beneath breaking bores in this study.

2.2 *Experimental flow conditions and bore generation*

The experiments were conducted with the same initially-steady water discharge: $Q = 0.05$ m^3/s and initial water depth $d_0 = 0.136$ m. The same initial flow conditions were used for both fixed and movable gravel bed configurations. With these conditions, the Shields number for the initially-steady flow was about 0.026, compared to a critical Shields number for the gravel material of 0.032.

The bore generation was induced by the rapid closure of the downstream tainter gate. After closure, the underflow gate opening ranged from 0 to 100 mm. By changing this opening, both breaking and undular bores could be generated with the same identical initial flow conditions. After gate closure, the bore propagated upstream. The acoustic displacement meters sampled non-intrusively the water surface elevation along the channel centreline, and the ADV sampling volume was located on the channel centreline at $x = 5$ m. For each experiment, the data acquisition was started 60 s prior to the bore generation. The gate closure took place in 0.1–0.15 s; this time is sufficiently small to be considered as instantaneous at the scale of the flow. Each experiment was stopped once the bore reached the channel upstream end. Note that the gate was similar to that used by Koch and Chanson (2009) and Docherty and Chanson (2012).

The experimental flow conditions are summarized in Table 1. The present experiments were performed with a relatively large initially-steady flow rate, hence a large Reynolds number. The main features were (a) a physical study of tidal bore propagation over a mobile bed, initially immobile in steady flow, and (b) the

Table 1 Physical studies in bores and positive surges

Reference	Q (m^3/s)	d_0 (m)	U (m/s)	F	Channel bed	Instrument (sampling rate)	Remarks
(1)	(2)	(3)	(4)	(5)	(6)	(7)	(8)
Hornung *et al.* (1995)	0	–	–	1.5–6	Smooth	PIV (15 Hz)	Rectangular channel
Koch and Chanson (2009)	0.040	0.079	0.14–0.68	1.3–2.0	Smooth PVC	ADV (50 Hz)	$B = 0.5$ m
Chanson (2010)	0.058	0.137	0.56–0.9	1.17–1.5	Smooth PVC	ADV (200 Hz)	$B = 0.5$ m
		0.142	0.50–0.9	1.1–1.5	Rough plastic screens		
Docherty and Chanson (2012)	0.05	0.118	0.26–0.85	1.08–1.59	Smooth PVC	ADV (200 Hz)	$B = 0.5$ m
		0.125	0.31–0.89	1.01–1.52	Fixed gravel bed		
Present study	0.05	0.136	0.4–0.9	1.05–1.4	Fixed gravel bed	Displacement meters (50 Hz)	$B = 0.5$ m
	0.052	0.136	0.63	1.19	Fixed gravel bed	Displacement	Undular bore
	0.050		0.87	1.39		meters and ADV	Breaking bore
	0.050		0.61	1.17	Movable gravel bed	(200 Hz)	Undular bore
	0.051		0.87	1.40			Breaking bore

Notes: B, channel width; d_0, initial water depth; F, bore Froude number; Q, initially-steady flow rate; U, bore celerity; (–), data not available. All experiments were conducted with tap water.

systematic comparison of the unsteady flow properties between fixed and mobile bed configurations, all other parameters being identical.

The channel flow conditions may be compared with tidal bore conditions by the application of a Froude similarity in the quasi-steady flow frame of reference in translation with the bore front.

3 Flow patterns, free-surface properties and sediment motion

The water surface measurements and visual observations were conducted for both fixed and movable bed configurations with similar initial conditions ($Q = 0.05$ m^3/s, $d_0 = 0.136$ m) and a range of Froude numbers F (Table 1). Undular bores were observed for the smallest Froude numbers ($1 < \mathsf{F} < 1.3$) (Fig. 2a). The front of the bore had a smooth shape and was followed by a train of well-defined undulations. Figure 2(a) presents a sequence of six shots illustrating the upstream propagation of the first and second wave crests. For Froude numbers between 1.2 and 1.3, some slight breaking was observed at the first wave crest. At the largest Froude numbers ($\mathsf{F} > 1.3$–1.4), a breaking bore was observed (Fig. 2b). The bore had a marked quasi-two-dimensional roller as seen based upon visual observations, high-shutter speed photographs and video movies. Its upstream propagation was characterized by the production of large-scale vortices with horizontal axis perpendicular to the bore direction. Figure 2(b) shows a series of photographs presenting the upstream advance of the breaking bore. The same flow patterns were observed on both fixed and movable gravel beds, and Fig. 2 presents some photographs of bores on movable gravel bed.

The flow properties in front of and behind the bore must satisfy the equations of continuity and momentum (Liggett 1994, Chanson 2012). For a rectangular flat channel, the ratio of conjugate depths d_{conj}/d_0 equals:

$$\frac{d_{conj}}{d_0} = \frac{1}{2}\left(\sqrt{1 + 8\mathsf{F}^2} - 1\right) \quad (2)$$

where d_{conj} is the flow depth behind the bore and F is the bore Froude number (Eq. 1). Despite some data scatter, the present physical data compared relatively well with Eq. (2) (Fig. 3a). In Fig. 3(a), the data are further compared with earlier studies on smooth and rough beds, and field data (see details in figure caption). For both undular and breaking bore experiments, Appendix lists the ratio of conjugate depths d_{conj}/d_0, the relative wave crest height d_{max}/d_0, the relative wave amplitude a_w/d_0 and wave steepness a_w/L_w, where a_w and L_w are, respectively, the wave amplitude and length of the first wave length.

The free-surface properties of undular bores were compared with previous studies (Fig. 3). These included the maximum depth d_{max} at the first wave crest, the wave steepness a_w/L_w and wave length. The present data are shown in a dimensionless form in Fig. 3(b)–(d), as the ratio of conjugate depth d_{conj}/d_0, the maximum depth d_{max}/d_0 at the first wave crest, the wave steepness a_w/L_w and wave length L_w/d_0 as functions of the bore Froude number.

In Fig. 3(b), the data are compared with the maximum height of a solitary wave (dashed line). The present data indicated an increase in wave height with increasing Froude number up to $\mathsf{F} = 1.25$–1.3, and a constant maximum height for $\mathsf{F} > 1.3$. It is believed that the maximum height was limited by the appearance of some breaking at the first wave crest. The wave steepness increased monotonically with increasing Froude number until the appearance of wave breaking ($\mathsf{F} \sim 1.3$). For larger Froude number, the data tended to decrease with increasing F (Fig. 3c). The wavelength decreased with increasing Froude number and the data were relatively close to a solution of the Boussinesq equation (Fig. 3d).

The present results showed some comparable data trends for bores on both smooth and rough beds, and the finding is consistent with the earlier findings of Chanson (2010). Altogether the results emphasized the effects of wave breaking at the first wave crest on the undular flow properties.

During the mobile gravel bed experiments, the sediment particle motion was recorded with the video camera. Altogether

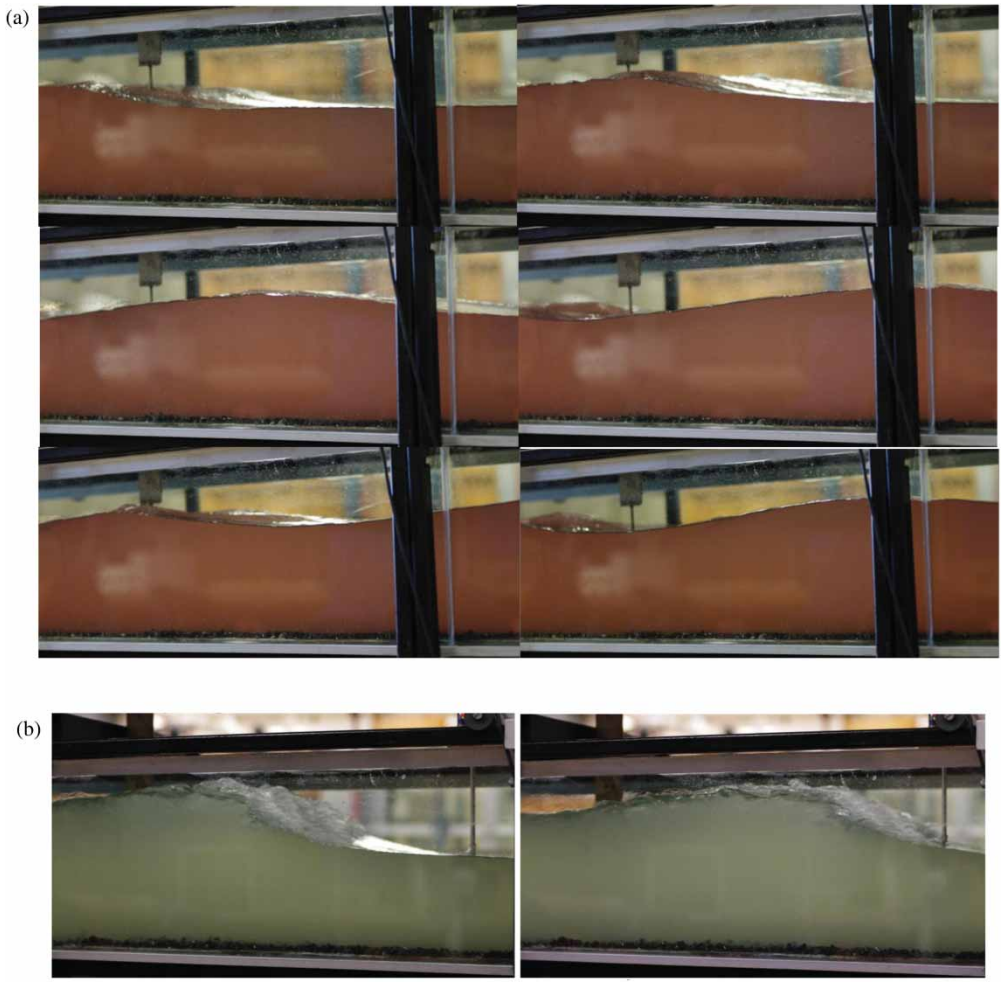

Figure 2 Undular and breaking bores on movable gravel bed – Bore propagation from left to right. (a) Undular bore propagating upstream ($\mathsf{F} = 1.2, Q = 0.050\,\mathrm{m^3/s}, d_0 = 0.136\,\mathrm{m}$, shutter speed: 1/80 s) – from left to right, top to bottom, $t = t_1, t_1 + 0.38\,\mathrm{s}$, $t_1 + 0.77$ s, $t_1 + 1.15, t_1 + 1.73, t_1 + 2.5\,\mathrm{s}$. (b) Breaking bore propagating upstream ($\mathsf{F} = 1.4, Q = 0.051\,\mathrm{m^3/s}$, $d_0 = 0.136\,\mathrm{m}$, shutter speed: 1/80 s) –from left to right, top to bottom, $t = t_2, t_2 + 0.19\,\mathrm{s}$

more than 50 video movies were taken. Prior to the tidal bore, no gravel bed motion was observed. During the undular bore experiments ($\mathsf{F} < 1.3$), the sediment movement was negligible. For each video, at most two sediment particles would move shortly, typically for less than 0.1 s. This was mostly some form of particle rotation rather than a change of absolute position. Basically, no particle motion was observed in the initially-steady flow and beneath undular bores.

On the other hand, some strong sediment motion was seen beneath breaking bores. During the breaking tidal bore experiments ($\mathsf{F} > 1.3$–1.4), a large number of particles were set into motion by the bore and moved upstream behind the bore front. The particle motion was by sliding and rolling. There was no sediment suspension. The visual appearance of the transient sediment motion was similar to a transient sheet flow. The physical observations demonstrated that the inception of gravel motion was associated mostly, although not always, with the passage of the roller toe (Point 2, Fig. 4a) as illustrated in Fig. 4(b). Figure 4(b) shows the trajectory of several gravel particles beneath a breaking bore during a single event; each particle is listed with a letter (A to O), the horizontal scale corresponds to 0.50 m and the coordinate X is positive upstream. Figure 4(b) includes also the passage of the characteristic features of the breaking bore as thick lines: Points 1, 2 and 3 (Fig. 4a). Each gravel particle trajectory includes the start and end points of the particle path. For the experiment shown in Fig. 4, the upstream particle velocity during the bore passage was 0.13 m/s on average. For comparison, the observed bore celerity was $U = 0.87$ m/s (Table 1). The particle trajectory data showed a number of particle behaviours. Some particles were advected upstream very rapidly: e.g. particles B, G, H in Fig. 4(b). A majority of the particles were convected upstream at a slower rate. For example, particles A, C, F in Fig. 4(b).

Visually the breaking bore passage induced a bed load sheet motion, although of a short duration. For example, in Fig. 4(b), the typical particle motion lasted between 0.2 and 0.4 s. While this study focused on the upstream sediment advection, the video recording analyses showed relatively little transverse motion of particles. Most particles were advected upstream behind the bore front.

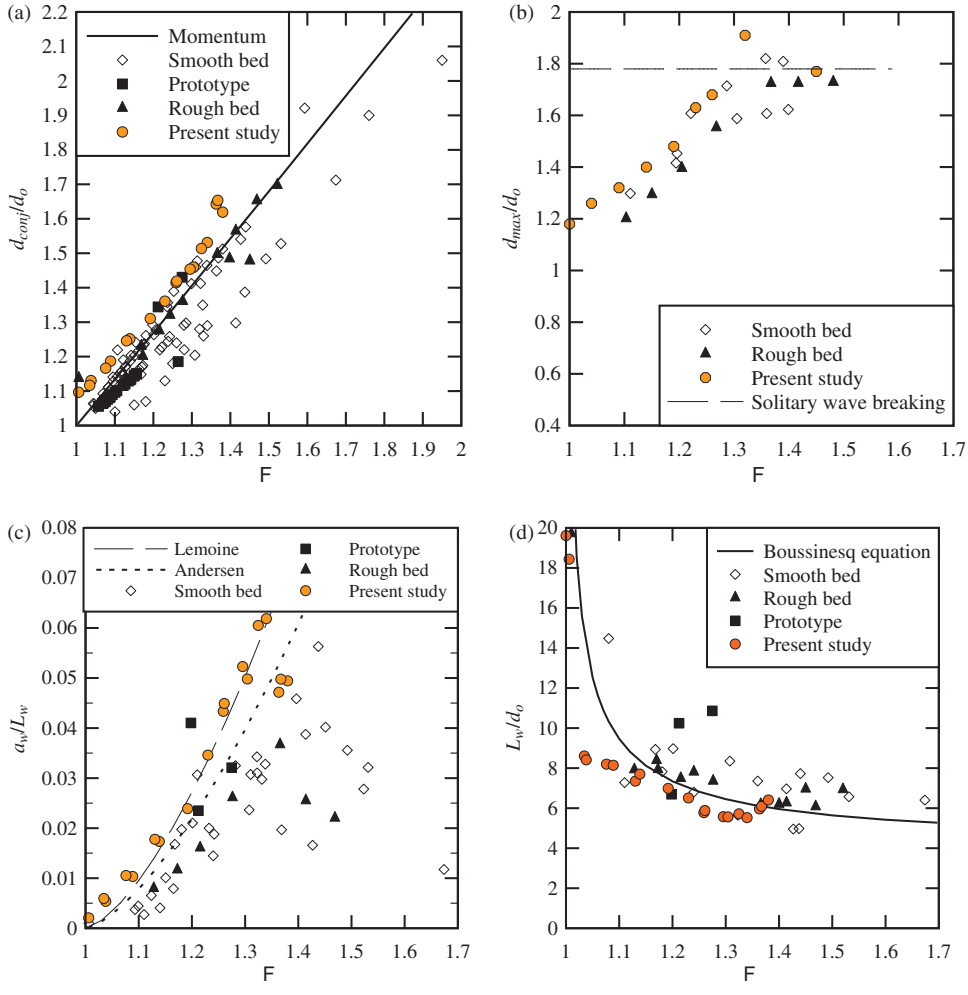

Figure 3 Dimensionless free-surface properties of tidal bores – data comparison between smooth bed (Benet and Cunge 1971, Favre 1935, Treske 1994, Koch and Chanson 2009, Chanson 2010, Docherty and Chanson 2012), rough bed data (Chanson 2010, Docherty and Chanson 2012, Present study (fixed gravel)) and prototype data (Benet and Cunge 1971, Lewis 1972, Navarre 1995, Wolanski *et al.* 2004) – wave steepness data are compared with the theories of Lemoine (1948) and Andersen (1978). (a) Ratio of conjugate depths d_{conj}/d_0. (b) Maximum depth d_{max}/d_0 at first undular wave crest. (c) Wave steepness a_w/L_w of undular bores. (d) Dimensionless wave length L_w/d_0 of undular bores

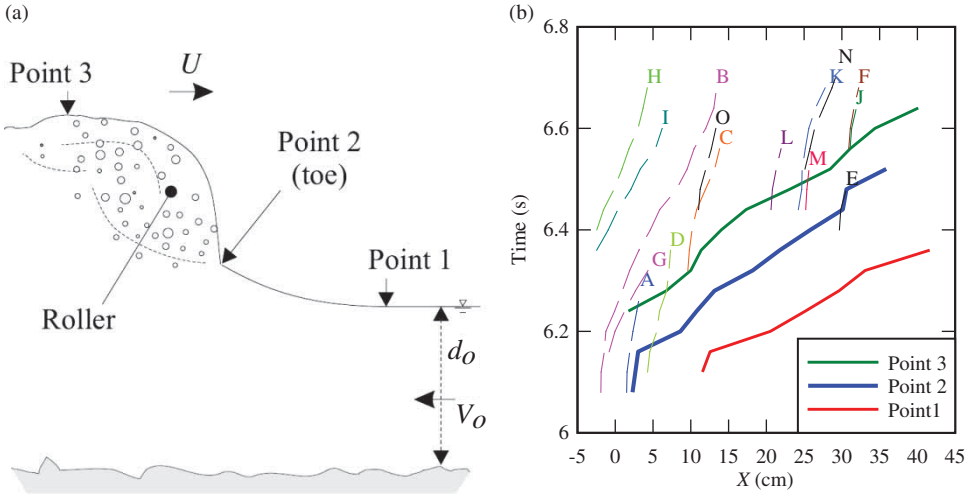

Figure 4 Gravel particle motion beneath a breaking bore – data: $Q = 0.051\ m^3/s$, $F = 1.4$, Video run 14. (a) Definition sketch. (b) Gravel particle trajectories as functions of time

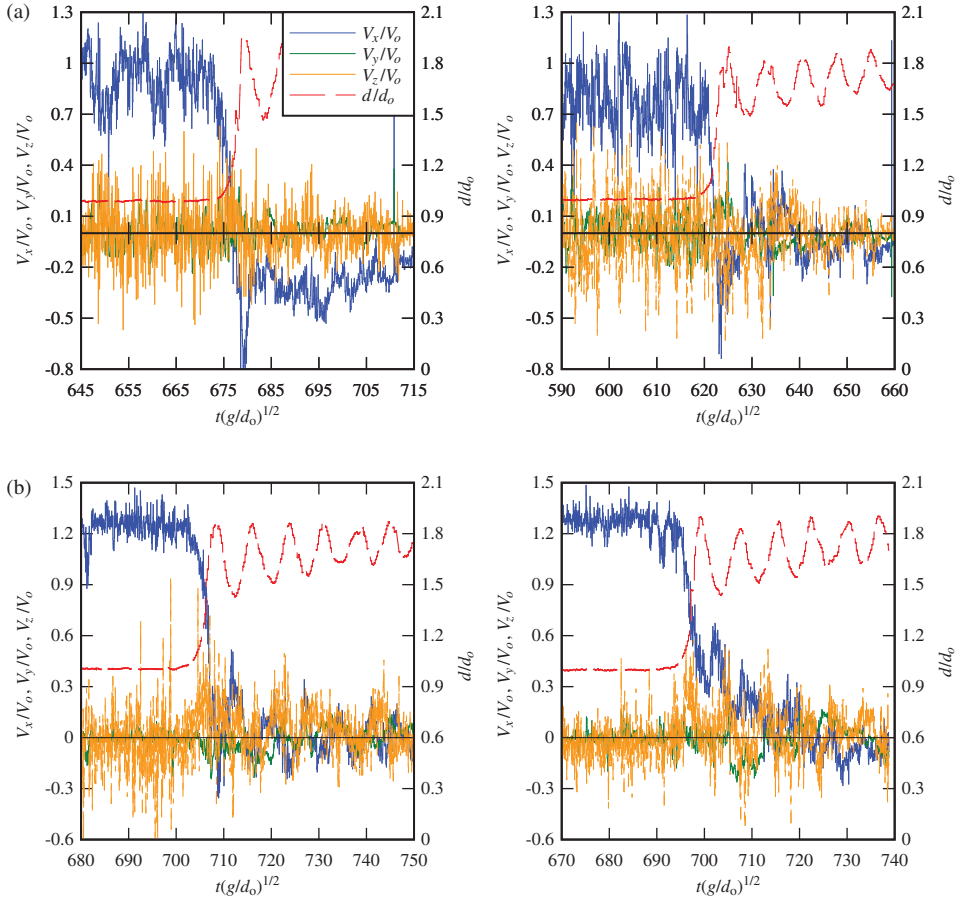

Figure 5 Instantaneous velocities beneath a breaking bore on fixed and mobile beds – data: $Q = 0.05\,\mathrm{m}^3/\mathrm{s}$, $\mathsf{F} = 1.4$. (a) $z/d_0 = 0.14$ – fixed bed (Left) and mobile bed (Right). (b) $z/d_0 = 0.69$ – fixed bed (Left) and mobile bed (Right)

4 Unsteady velocity properties above fixed and movable boundary

The instantaneous velocity components were sampled at $x = 5$ m with both fixed and movable gravel bed configurations at several vertical elevations z (Table 1). Figure 5 presents some typical results in terms of the water elevation above the bed and instantaneous velocity components for a breaking bore. The graphs were obtained for a similar Froude number F at the same relative elevation z/d_0, but for the two types of bed configurations, i.e. fixed and mobile. Herein, V_x, V_y and V_z were positive, respectively, downstream, towards the left sidewall and upwards.

Beneath the undular bore, the longitudinal velocity component decreased when the bore front passed above the sampling volume (data not shown). After the bore, the longitudinal velocity was typically positive at all vertical elevations, being minimum beneath the wave crests and oscillating with the same period as the surface undulations (e.g. seen in Fig. 2a) but out of phase as expected by the ideal fluid flow theory. The vertical velocity data presented a similar oscillating pattern beneath the surface undulations. Both patterns may be derived from irrotational flow considerations (Rouse 1938, Montes and Chanson 1998). The present findings were identical for both fixed and mobile gravel beds, and they were similar to earlier results (Koch and Chanson 2008).

With a breaking bore, the propagation of the roller was associated with a rapid rise of the water surface during the breaking roller passage followed by some residual undulations for $\mathsf{F} = 1.4$ (Fig. 5). The propagation of the bore roller was linked with a strong longitudinal deceleration and some positive vertical velocities for a short period of time, as reported by Hornung *et al.* (1995) and Koch and Chanson (2009). The former effect is clearly seen in Fig. 5, while the latter is illustrated in Fig. 6. Figure 6 shows the vertical velocity component during the breaking bore passage together with the low-pass filtered data. Figure 7 presents the maximum instantaneous vertical velocities at several relative elevations z/d_0. Both fixed and mobile bed configuration data are shown. The results are compared with the ensemble-averaged data of Docherty and Chanson (2012), and an inviscid solution of the Boussinesq equation (Montes and Chanson 1998) calculated from the observed free-surface curvature immediately upstream of the roller toe. The data of Docherty and Chanson (2012) were averaged over 20 runs and the results illustrated some key differences between smooth bed and rough bed data. Indeed, the theoretical results were close to the smooth bed data but differed from the observations above fixed gravel bed, hinting the limitations of the inviscid solution for bores propagating over rough gravel bed. Despite some obvious difference between instantaneous maximum and ensemble-averaged data,

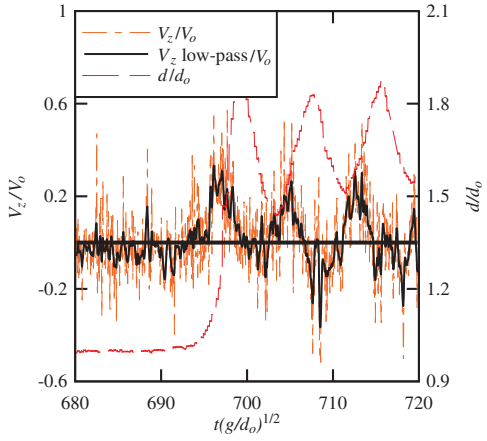

Figure 6 Vertical velocity component beneath a breaking bore: instantaneous and low-pass filtered data (cut-off frequency: 2 Hz) – flow conditions: $Q = 0.05\,m^3/s$, $F = 1.4$, $z/d_0 = 0.69$, fixed bed

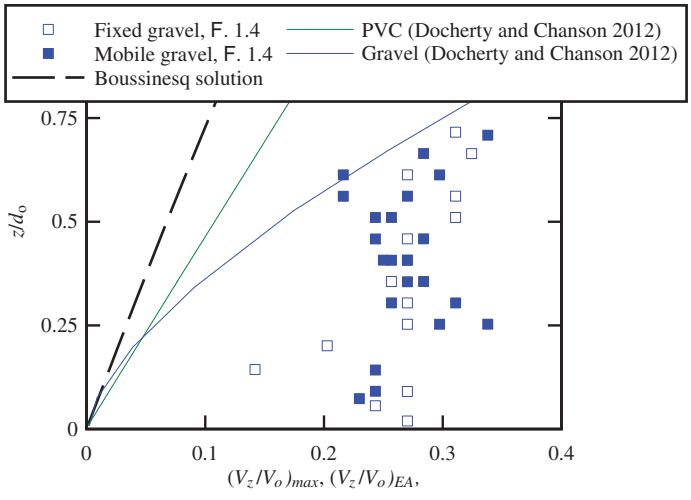

Figure 7 Maximum instantaneous vertical velocity beneath a breaking bore roller on mobile and fixed gravel beds – comparison with some ensemble-averaged data (Docherty and Chanson 2012, $F = 1.5$) and an inviscid Boussinesq equation solution calculated from the measured free-surface profile

the general data trend was consistent. They emphasized the existence of an upward momentum flux during the breaking bore front passage (Fig. 7).

The experimental data highlighted the existence of a transient recirculation next to the bed beneath the breaking bore: that is, the longitudinal flow deceleration ended with a negative longitudinal velocity component $V_x < 0$ as illustrated in Fig. 5(a): e.g. for $t(g/d_0)^{1/2} \sim 680$ in Fig. 5(a) (Left). For the same Froude number and same relative elevation z/d_0, the longitudinal velocity on mobile bed did not reach the maximum instantaneous negative velocities observed on the fixed bed (Fig. 5). This is seen in Fig. 5(a) next to the bed and in Fig. 5(b) at a higher relative elevation. The finding could be linked to some energy dissipation in the form of energy transfer to initiate the motion of gravel particles behind the bore, as indeed the passage of the breaking bore was associated with some upstream gravel bed motion (Section 4). In a dam-break wave, Carrivick *et al.* (2011) observed similarly a greater rate of energy dissipation on mobile bed compared with a fixed bed configuration.

Close to the bed, the negative transient recirculation velocities were larger with both mobile and fixed bed configurations than those observed on smooth bed (Koch and Chanson 2009). The findings were consistent with the results of Chanson (2010) and Docherty and Chanson (2012) on fixed beds. They tended to imply that the transient recirculation was strongly linked to the boundary friction, as shown by recent numerical results (Furuyama and Chanson 2010, Lubin *et al.* 2010). Some large vertical velocity fluctuations were observed shortly after the bore passage.

In the unsteady bore flow, the Reynolds stress tensor was calculated using a variable interval time averaging technique (Garcia and Garcia 2006, Koch and Chanson 2008). A number of data (including present data) showed relatively small quantitative differences in turbulence levels, beneath the bore front, between undular and breaking surges for the same initially-steady flow rate. On the other hand, the same data highlighted some major change in shear stress pattern associated with a pseudo-periodic loading beneath undulations (undular data, not shown).

Different patterns in Reynolds stress fluctuations were observed before and after the breaking bore passage (Fig. 8). In the initially-steady flow on the rough gravel bed, the Reynolds stress components exhibited significant fluctuations close to the bed and the fluctuations decreased with increasing elevation. During a short period corresponding to the bore front passage, some large fluctuations were observed for all components of the Reynolds stress tensor (Fig. 8). For example, for $t(g/d_0)^{1/2}$ between 635 and 650 in Fig. 8. While Fig. 8 presents some data at a single elevation, the same trend was observed throughout the entire water column. Some short periods of high Reynolds stresses were observed shortly after the breaking bore passage. Similar patches of turbulence were reported by Wolanski *et al.* (2004), Simpson *et al.* (2004) and Mouaze *et al.* (2010) in the field, as well as in the numerical results of Lubin *et al.* (2010).

The medians of normal Reynolds stress components were calculated to compare the impact of the breaking bore on fixed and mobile beds. During the bore propagation, the normal Reynolds stress components and turbulent kinetic energy (TKE) were systematically 10–30% higher on the mobile bed than on the fixed bed, at the same relative bed elevation and for the same Froude number (Table 2). The results were observed throughout the water column and some quantitative data are reported in Table 2. The findings were consistent with the results of Nakato *et al.* (1977) in oscillatory flows in a U-tube, although some steady flow data suggested a different trend (Dey *et al.* 2011). It is thought that the present results highlighted the complex interactions between mobile bed and unsteady flow turbulence.

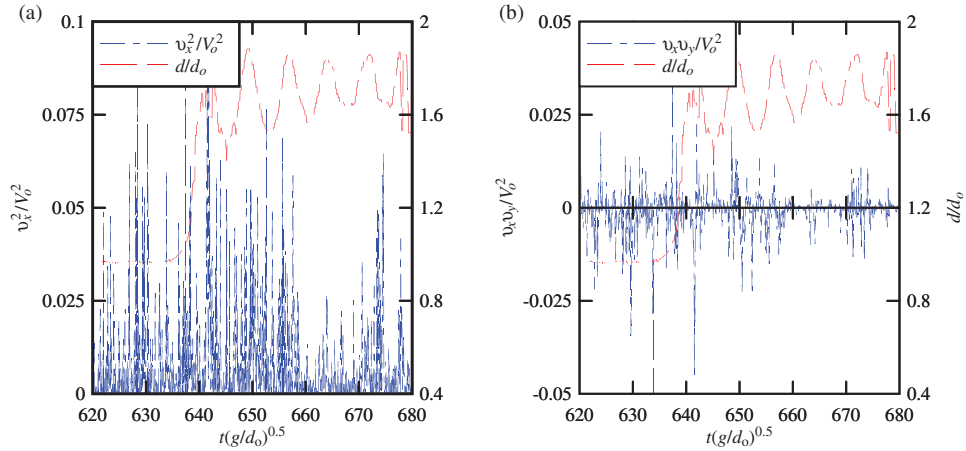

Figure 8 Time variations of dimensionless Reynolds stresses v_x^2/V_0^2 and $v_x v_y/V_0^2$ beneath a breaking bore roller on mobile gravel bed – data: $Q = 0.05\,m^3/s$, F = 1.4, mobile gravel bed, $z/d_0 = 0.36$. (a) Water depth and normal stress v_x^2/V_0^2. (b) Water depth and tangential stress $v_x v_y/V_0^2$

Table 2 Experimental measurements of normal Reynolds stresses and TKE beneath breaking tidal bores – Median values

				Median value			
Q (m^3/s)	F	z/d_0	Channel bed	v_x^2/V_0	v_y^2/V_0	v_z^2/V_0	TKE$/V_0$
(1)	(2)	(3)	(4)	(5)	(6)	(7)	(8)
0.05	1.4	0.25	mobile	0.0021	0.0006	0.0051	0.0063
			fixed	0.0018	0.0004	0.0040	0.0053
		0.30	mobile	0.0026	0.0007	0.0064	0.0077
			fixed	0.0019	0.0004	0.0044	0.0069

Note: TKE $= 0.5(v_x^2 + v_y^2 + v_z^2)$.

5 Discussion

The physical data demonstrated a strong transient gravel bed load transport during the breaking bore propagation, although no sediment motion was observed in the initially-steady flow or beneath the undular bores, for the same initial flow rate. For a mobile layer sheet flow, Sleath (2000) introduced a dimensionless number S defined as the ratio of particle acceleration to the reduced gravity acceleration:

$$S = \frac{(\text{Particle acceleration})_{max}}{\frac{\rho_s - \rho}{\rho} g} \quad (3)$$

In this study, the maximum particle acceleration was observed along the x-direction. For the data shown in Fig. 4(b), the maximum acceleration was about $5\,m/s^2$ on average. Altogether this yielded a dimensionless parameter S about 0.3, for which the assumption of quasi-steady sediment transport rate is invalid in the mobile layer (Sleath 2000).

Physically, for a particle initially fixed on the bed, the propagation of the breaking bore was associated with a combination of several de-stabilizing processes including a highly turbulent motion, a longitudinal pressure gradient, and some transient upward irrotational velocity linked with ideal fluid flow motion. The larger flow depth behind the bore implies a positive pressure gradient $\partial P/\partial x$ close to the bed that is proportional in first approximation to: $\partial P/\partial x \propto \rho g\ (d_{conj} - d_0) \propto (F - 1)$. The pressure gradient is proportional to the free-surface slope. A key difference between undular and breaking bore is the flow discontinuity at the roller toe where the local free-surface curvature is infinite. Since the observations showed the onset of sediment motion at the roller toe passage, it is thought that the longitudinal pressure might play a dominant role in the sediment motion inception. With the irrotational motion, the free-surface is a streamline and the upstream bore propagation was characterized by an upward streamline curvature, hence a rapid pressure and velocity redistributions including a transient positive vertical velocity (Figs. 6 and 7) which might add to the particle destabilization. Turbulence shear contributed further to a drag force acting in the upstream direction during the transient recirculation seen in Fig. 5(a). For example, for the data shown in Figs. 4(b) and 5(a), the maximum acceleration force was about 1.3×10^{-3} N per particle, while the longitudinal pressure gradient force was about 5.9×10^{-4} N on average per particle and the maximum drag force was less than 6×10^{-4} N per particle. All these processes added together and contributed to the gravel bed load inception and upstream advection of gravel particles behind the bore front.

The present observations highlighted that the gravel bed load motion was initiated primarily by the passage of the roller toe (Fig. 4). The finding would tend to support the predominant roles of the highly turbulent motion beneath the bore roller and the effects of unsteady pressure gradient. The former effect was documented numerically by Lubin *et al.* (2010) showing the generation of large-scale vortices beneath the breaking bore front and their advection behind the bore front. The latter effect was discussed by Lighthill (1978), but both theoretical and numerical approaches need further physical validation.

6 Conclusions

The turbulent velocity characteristics beneath both undular and breaking bores were investigated physically on two types of gravel bed: fixed and movable. This study was aimed at simplifying the entire sedimentary processes in tidal bore-affected estuaries and focused on a simple study based upon a Froude dynamic similarity in terms of the hydrodynamics. The sediment material and its properties (density, size) were selected to observe no sediment motion in the initially-steady flow and some onset of sediment transport under (breaking) bores. Some complementary instrumentation (displacement metres, ADV, video camera) were used to record the unsteady turbulent flow motion during the tidal bore propagation and its impact in terms of gravel bed motion.

The physical observations showed that the undular bore had a negligible effect on gravel particle movement, but a large amount of gravel particles were set into motion beneath the breaking bore front and advected upstream in a bed load motion. The data showed an intense transient sheet flow motion of sliding and rolling particles beneath the breaking roller. The gravel particles were de-stabilized by the roller toe passage and advected in bed load motion behind the bore. The results pointed to the predominant role of the unsteady pressure gradient and highly turbulent motion beneath the bore roller.

The velocity measurements were performed at different vertical elevations using acoustic Doppler velocimetry with high temporal resolution (200 Hz). The data showed some basic differences between fixed and movable gravel bed configurations. With a breaking bore, the turbulent velocity data indicated that, with similar flow conditions and relative elevation ($\mathsf{F}, z/d_0$), the magnitude of negative transient longitudinal velocity close to the bed was greater on fixed bed than on mobile bed. The negative transient recirculation velocities were, however, largely close to the bed, highlighting the effect of boundary friction. The propagation of the breaking bore highlighted some instantaneous upwards momentum flux linked with the streamline curvature immediately upstream of the roller. During the bore passage, both normal Reynolds stresses and TKE were on average 10–30% higher on the mobile bed than on the fixed bed, at the same relative bed elevation for the same Froude number, and the results were observed throughout the entire water column.

It is known that the tidal bore propagation does have a major impact on the sediment processes in the estuarine zone. It is believed that the present investigation is the first physical study into the sediment motion under tidal bores. Future contributions on this topic should provide further details into the sediment suspension processes, including the impact of the change in bathymetry induced by the tidal bore propagation.

Acknowledgements

The authors thank Dr Pierre Lubin (University of Bordeaux) for his helpful advice. They acknowledge the technical assistance of Graham Illidge, Ahmed Ibrahim and Jason van der Gevel (University of Queensland).

Notation

a_w = amplitude of the first wave length (m)
B = channel width (m)
d = flow depth measured normal to the bed (m)
d_{max} = water depth of first wave crest (m)
d_0 = initial flow depth (m)
F = tidal bore Froude number: $\mathsf{F} = (V_0 + U)/\sqrt{g\ d_0}$
f = Darcy–Weisbach friction factor
g = gravity constant: $g = 9.80\,\mathrm{m/s^2}$ in Brisbane, Australia
L_w = wave length of the first wave length (m)
P = pressure (Pa)
Q = volume flow rate ($\mathrm{m^3/s}$)
TKE = turbulent kinetic energy ($\mathrm{m^2/s^2}$): $\mathrm{TKE} = 0.5(v_x^2 + v_y^2 + v_z^2)$
t = time (s)
U = bore front celerity (m/s)
V = velocity (m/s)
V_0 = initial flow velocity (m/s)
v = turbulent velocity fluctuation (m/s)
X = longitudinal co-ordinate positive upstream (m)
x = longitudinal distance measured from the channel upstream end (m)
z = particle elevation above the invert (m)
ρ = water density ($\mathrm{kg/m^3}$)
ρ_s = particle density ($\mathrm{kg/m^3}$)

Subscripts

conj = conjugate flow conditions
EA = ensemble-average
0 = initial flow conditions prior to the bore passage
x = longitudinal component
y = transverse component
z = vertical component

References

Andersen, V.M. (1978). Undular hydraulic jump. *J. Hydraulic Div.* 104(HY8), 1185-1188. Discussion: 105(HY9), 1208–1211.

Benet, F., Cunge, J.A. (1971). Analysis of experiments on secondary undulations caused by surge waves in trapezoidal channels. *J. Hydraulic Res.* 9(1), 11–33.

British Standard (1943). *Flow measurement. British Standard Code BS 1042:1943*. British Standard Institution, London.

Carrivick, J.L., Jones, R., Keevil, G. (2011). Experimental insights on geomorphological processes within dam break outbursts floods. *J. Hydrol.* 408, 153–163.

Chanson, H. (2010). Unsteady turbulence in tidal bores: The effects of bed roughness. *J. Waterway Port Coastal Ocean Eng.* 136(5), 247–256.

Chanson, H. (2012). Momentum considerations in hydraulic jumps and bores. *J. Irrigat. Drain. Eng.* 138(4), 382–385.

Chanson, H., Tan, K.K. (2010). Turbulent mixing of particles under tidal bores: An experimental analysis. *J. Hydraulic Res.* 48(5), 641–649.

Chanson, H., Reungoat, D., Simon, B., Lubin, P. (2011). High-frequency turbulence and suspended sediment concentration measurements in the Garonne river tidal bore. *Estuar. Coastal Shelf Sci.* 95(2–3), 298–306.

Chen, J., Liu, C., Zhang, C., Walker, H.J. (1990). Geomorphological development and sedimentation in Qiantang estuary and Hangzhou bay. *J. Coastal Res*. 6(3), 559–572.

Darwin, G.H. (1897). The tides and Kindred phenomena in the solar system. *Lectures delivered at the Lowell Institute*, Boston, W.H. Freeman and Co. Publishers, London, 1962.

Dey, S., Sarkar, S., Solari, L. (2011). Near-bed turbulence characteristics at the entrainment threshold of sediment beds. *J. Hydraulic Eng.* 137(9), 945–958.

Docherty, N.J., Chanson, H. (2012). Physical modelling of unsteady turbulence in breaking tidal bores. *J. Hydraulic Eng.* 138(5), 412–419.

Favre, H. (1935). Etude Théorique et Expérimentale des Ondes de Translation dans les Canaux Découverts. (Theoretical and experimental study of travelling surges in open channels.) Dunod, Paris, France (in French).

Furuyama, S., Chanson, H. (2010). A numerical solution of a tidal bore flow. *Coastal Eng.* 52(3), 215–234.

Garcia, C.M., Garcia, M.H. (2006). Characterization of flow turbulence in large-scale bubble-plume experiments. *Exp. Fluids* 41(1), 91–101.

Graf, W.H. (1971). *Hydraulics of sediment transport*. McGraw-Hill, New York, USA.

Henderson, F.M. (1966). *Open channel flow*. MacMillan Company, New York, USA.

Hornung, H.G., Willert, C., Turner, S. (1995). The flow field downstream of a hydraulic jump. *J. Fluid Mech.* 287, 299–316.

Koch, C., Chanson, H. (2008). Turbulent mixing beneath an undular bore front. *J. Coastal Res.* 24(4), 999–1007.

Koch, C., Chanson, H. (2009). Turbulence measurements in positive surges and bores. *J. Hydraulic Res.* 47(1), 29–40.

Lemoine, R. (1948). Sur les Ondes Positives de Translation dans les Canaux et sur le Ressaut Ondulé de Faible Amplitude. (On the positive surges in channels and on the undular jumps of low wave height.) *Jl La Houille Blanche*, March–April, 183–185 (in French).

Lewis, A.W. (1972). Field studies of a tidal bore in the River Dee. *M.Sc. thesis*, Marine Science Laboratories, University College of North Wales, Bangor, UK.

Liggett, J.A. (1994). *Fluid mechanics*. McGraw-Hill, New York, USA.

Lighthill, J. (1978). *Waves in fluids*. Cambridge University Press, Cambridge, UK.

Lubin, P., Chanson, H., Glockner, S. (2010). Large eddy simulation of turbulence generated by a weak breaking tidal bore. *Environ. Fluid Mech.* 10(5), 587–602.

Montes, J.S., Chanson, H. (1998). Characteristics of undular hydraulic jumps. Results and calculations. *J. Hydraulic Eng.* 124(2), 192–205.

Mouaze, D., Chanson, H., Simon, B. (2010). Field measurements in the tidal bore of the Sélune River in the bay of Mont Saint Michel (September 2010). *Hydraulic Model Report No. CH81/10*, School of Civil Engineering, The University of Queensland, Brisbane, Australia.

Nakato, T., Locher, F.A., Glover, J.R., Kennedy, J.F. (1977). Wave entrainment of sediment from rippled beds. *J. Waterway Port Coastal Ocean Div.* 103(WW1), 83–99.

Navarre, P. (1995). Aspects Physiques du Caractère Ondulatoire du Macaret en Dordogne. (Physical features of the undulations of the Dordogne River tidal bore.) *D.E.A. thesis*, University of Bordeaux, France (in French).

Nikora, V., Goring, D. (2000). Flow turbulence over fixed and weakly mobile gravel bed. *J. Hydraulic Eng.* 126(9), 679–690.

Peregrine, D.H. (1966). Calculations of the development of an undular bore. *J. Fluid Mech.* 25, 321–330.

Rayleigh, L. (1908). Note on tidal bores. *Proc. Royal Soc. of London*, 81(541), 448–449.

Rouse, H. (1938). *Fluid mechanics for hydraulic engineers*. McGraw-Hill Publisher, New York, USA.

Simpson, J.H., Fisher, N.R., Wiles, P. (2004). Reynolds stress and TKE production in an estuary with a tidal bore. *Estuar. Coastal Shelf Sci.* 60(4), 619–627.

Sleath, J.F.A. (2000). Ripple geometry under severe wave conditions. Proc. 27th Int. Conf. *Coastal Engineering*, Sydney, Australia, 2686–2699.

Tessier, B., Terwindt, J.H.J. (1994). An example of soft-sediment deformations in an intertidal environment – the effect of a tidal bore. *Comptes-Rendus de l'Académie des Sciences, Série II* 319(2), 217–233 (in French).

Treske, A. (1994). Undular bores (Favre-Waves) in open channels – experimental studies. *J. Hydraulic Res.* 32(3), 355–370. Discussion: 33(3), 274–278.

Tricker, R.A.R. (1965). *Bores, breakers, waves and wakes*. American Elsevier Publishers Co., New York, USA.

Wolanski, E., Williams, D., Spagnol, S., Chanson, H. (2004). Undular tidal bore dynamics in the Daly Estuary, Northern Australia. *Estuar. Coastal Shelf Sci.* 60(4), 629–636.

Appendix

Table A1 Free-surface properties of bores on fixed gravel bed

Bore type	Q (m^3/s)	d_0 (m)	V_0 (m/s)	U (m/s)	F	d_{conj}/d_0	d_{max}/d_0	a_w/d_0	a_w/L_w
(1)	(2)	(3)	(4)	(5)	(6)	(7)	(8)	(9)	(10)
Breaking	50.2	0.136	0.73	0.86	1.36	1.64	N/A	N/A	N/A
	50.1	0.136	0.74	0.84	1.37	1.65	N/A	N/A	N/A
Undular	50.1	0.136	0.74	0.79	1.32	1.51	1.91	0.35	5.72
	50.1	0.136	0.76	1.3	1.45	1.77	0.29	0.29	5.57
	50	0.136	0.7	0.73	1.26	1.41	1.68	0.25	5.78
	50	0.136	0.74	0.68	1.23	1.36	1.63	0.23	6.51
	50	0.136	0.74	0.63	1.19	1.31	1.48	0.17	6.99
	50	0.136	0.74	0.58	1.14	1.25	1.4	0.13	7.7
	50	0.136	0.74	0.52	1.09	1.19	1.32	0.08	8.14
	50	0.136	0.74	0.45	1.04	1.13	1.26	0.05	8.41
	50	0.136	0.74	0.41	1	1.1	1.18	0.04	19.62

Notes: d_0, initial water depth; d_{conj}, conjugate depth; d_{max}, water depth of first wave crest; F, tidal bore Froude number; a_w, wave amplitude of first wave length; L_w, first wave length; Q, water discharge. All data were recorded at $x = 5$ m.